Applied Physics B (2023) 129:177
https://doi.org/10.1007/s00340-023-08122-8

Applied Physics B
Lasers and Optics

RESEARCH

Dual-band light-induced thermoelastic spectroscopy utilizing an antiresonant hollow-core fiber-based gas absorption cell

Piotr Bojęś[1] · Piotr Jaworski[1] · Piotr Pokryszka[1] · Walter Belardi[2] · Vincenzo Spagnolo[3] · Karol Krzempek[1]

Received: 10 July 2023 / Accepted: 29 September 2023 / Published online: 24 October 2023

Abstract
In this paper, dual-band gas detection using a combination of the light-induced thermoelastic spectroscopy (LITES) and an antiresonant hollow-core fiber-based (ARHCF) gas absorption cell is demonstrated. The broad wavelength operation capability of a standard 32 kHz quartz tuning fork and the self-developed fiber-based gas absorption cell was exploited to demonstrate quasi-simultaneous detection of N_2O and CO_2, at 4570 nm (2188.2 cm^{-1}) and 2006 nm (4985.9 cm^{-1}), respectively. The signal analysis was based on the wavelength modulation spectroscopy technique, allowing to achieve a noise equivalent absorption coefficient (NEA) of 8.6×10^{-7} cm^{-1} and 1.7×10^{-6} cm^{-1} for N_2O and CO_2, respectively. The results indicate that the combination of ARHCFs with the LITES method is well suited for the design of broadband gas detectors and show remarkable potential in the fabrication of miniaturized, versatile and relatively inexpensive gas sensors operating over a wide spectral range, thus allowing multigas detection.

1 Introduction

Laser absorption spectroscopy (LAS) has been known as a powerful, versatile and highly efficient technique for targeting molecular fingerprints of various gaseous substances, ranging from inert gases up to greenhouse, highly toxic and explosive substances [1–5]. LAS-based gas detectors in a vast majority rely on the use of narrow-linewidth, single-frequency laser sources with an operational wavelength range falling into the mid-infrared (mid-IR) spectral band [6]. The mid-IR spectral range is of high interest for the spectroscopic community; however, it is connected with several, nontrivial, requirements while developing gas detectors. Mid-IR provides access to the strong absorption features of molecules, the concentration of which needs to be precisely monitored from environmental, industrial, life protection and economic point of views, in most cases using sensors with sensitivity down to parts-per-billion in volume (ppbv) concentration level or even less [3]. As a result of these strict requirements and operation in the mid-IR spectral band, such sensors are typically built in configurations necessitating complex optical setups based on the use of multipass or cavity-enhanced cells, to provide long laser–gas sample interaction paths, and requiring sensitive mid-IR photodetectors [7, 8]. This results in bulky and expensive LAS-based systems, sensitive to mechanical vibrations and temperature drifts, thereby, limiting their out-of-laboratory applications. Therefore, researchers worldwide have focused their efforts on developing gas-sensing systems that could provide the required sensitivity while maintaining a non-complex, robust and cost-effective design. This entails finding an efficient and available of-the-shelf technology for detecting especially mid-IR laser radiation and reducing or even entirely eliminating bulk-optics-based components from the sensor architecture.

The first aspect of the problem of developing non-complex and efficient gas sensors can be addressed by implementing different non-semiconductor-based photodetectors. In a typical semiconductor-based photodetector, the internal photoelectric effect is used to measure the intensity of the detected light. These types of detectors are usually highly spectrally limited due to material characteristics. In addition, they sometimes require special working conditions, such as

✉ Piotr Bojęś
piotr.bojes@pwr.edu.pl

[1] Faculty of Electronics, Photonics and Microsystems, Wroclaw University of Science and Technology, Wybrzeże Wyspiańskiego 27, 50-370 Wrocław, Poland

[2] Université de Lille, CNRS, UMR 8523-PhLAM-Physique des Lasers, Atomes et Molécules, 59000 Lille, France

[3] PolySense Lab, Dipartimento Interateneo di Fisica, University and Politecnico of Bari, Via Amendola 173, Bari, Italy

low operating temperature, and their production process is connected with the use of highly toxic materials that are dangerous to human life and the environment [9]. Kosterev et al. have presented a significant step toward the development of a new efficient signal detection method [10], by successfully implementing a quartz tuning fork (QTF) as a sensitive optoacoustic detector. The QTF is a small quartz resonator that is commonly used in a wide variety of electronic devices for timing purposes. As a result of the piezoelectrical nature of quartz, the QTF generates an electrical signal if a mechanical stress or a photothermal effect is generated. Two main measurement techniques have been developed for absorption spectroscopy: quartz-enhanced photoacoustic spectroscopy (QEPAS) [10, 11] and light-induced thermoelastic spectroscopy (LITES) [12, 13]. In QEPAS, the QTF response is induced by heating the gas molecules with a laser beam in close vicinity to the QTF's prongs. As a result of this local gas heating, one can observe a local change in pressure. When the excitation laser beam is additionally modulated, e.g., with a sine wave signal, an acoustic wave is generated as a result of the aforementioned phenomenon [10]. Consequently, the acoustic waves hit the QTF prongs and deflect them, generating an electric signal, whose amplitude is proportional to the molecular concentration of the measured gas sample.

In LITES, the QTF is employed as a photodetector, via excitation by a local heating of its structure due to absorption of a sinusoidally modulated laser beam [13]. With light focused on the quartz, the material starts to heat up in the focal spot, and, via a thermoelastic effect, its structure in this area temporarily deforms. If the modulation frequency matches the QTF resonance frequency, the modulated thermal expansion of the material causes vibrations of the QTF, which leads to the generation of a measurable piezoelectric signal. The spectroscopic signal is encoded in the amplitude of the laser beam passing through a gas sample, before it is focused on the QTF. Furthermore, as a result of the absorption characteristic of the QTF material, this simple device can be easily used to detect laser radiation both in the near- and mid-IR spectral bands without additional modification of its structure, not possible with conventional semiconductor-based detectors, and in principle, significantly reducing the complexity and costs of the sensor [13].

QEPAS, despite the achievable lower detection limits in state-of-the-art setups, requires a more complex setup [11, 14]. LITES systems, on the other hand, have been shown to deliver high sensitivity with a more simple design of the sensing system, opening a new route for compact laser-based gas sensors [13, 15].

The second aspect in terms of the development of versatile, compact and efficient gas sensors is related to the methods of increasing the laser–gas molecules interaction path length, which is mandatory to obtain high sensitivity. An alternative and promising solution to commonly used MPCs has emerged with the development of novel, microstructured fibers, the so-called antiresonant hollow-core fibers (ARHCFs) [16–18]. ARHCFs, due to their unique structure and light guidance mechanism, enable efficient transmission of a laser beam over a few tens of meters length within its empty core [19]. Since the fiber core is empty, it is possible to fill it efficiently and relatively fast with a target gas sample. Therefore, a gas-filled ARHCF can form a versatile, low-volume and compact gas absorption cell that delivers an optical path with a length of up to a few tens of meters [19, 20]. Furthermore, ARHCFs are characterized by an excellent ability to simultaneously guide light in two significantly dissimilar spectral bands, e.g., in the near- and mid-IR [21, 22]. This opens a great opportunity for developing novel multigas sensors with greatly reduced complexity and volume and increased versatility. Up to date, several different ARHCF-aided gas sensors have been constructed based on the use of various spectroscopy techniques, e.g., tunable diode laser absorption spectroscopy (TDLAS) [23], wavelength modulation spectroscopy (WMS) [18, 24], dispersion spectroscopy [25] and photothermal spectroscopy (PTS) [26, 27] showing the capacity to reach detection limits at parts-per-trillion by volume (pptv) level [28]. However, the full potential of this novel approach to gas sensing has not been fully explored yet.

In this work, we present for the first time a successful demonstration of quasi-simultaneous multiple gas detection inside an ARHCF-based gas absorption cell combined with the LITES technique. The developed sensor utilized a self-fabricated ARHCF with a length of 1 m capable of transmitting with low-loss light at ~ 4.5 µm and ~ 2.0 µm. The system targeted simultaneously strong carbon dioxide (CO_2) and (N_2O) transitions in the near- and mid-IR spectral bands, respectively. The sensor configuration is based on the use of a minimum number of bulk-optics components and the spectroscopic signal retrieval is retrieved with the aid of a single QTF photodetector combined with a custom-made, low-noise electronics.

2 Materials

2.1 ARHCF and tuning fork

In the proposed sensor configuration, the gas absorption cell was based on a 1 m-long self-fabricated, all-silica ARHCF, the cross section of which is shown in Fig. 1a. The microstructured cladding was formed by eight circular capillaries with an average diameter and wall thickness of 60 µm and 1.5 µm, respectively. This translates to a total volume of ARHCF-based cell of only ~ 0.058 ml. Commercial absorption cells with an optical length of 1 m (Thorlabs,

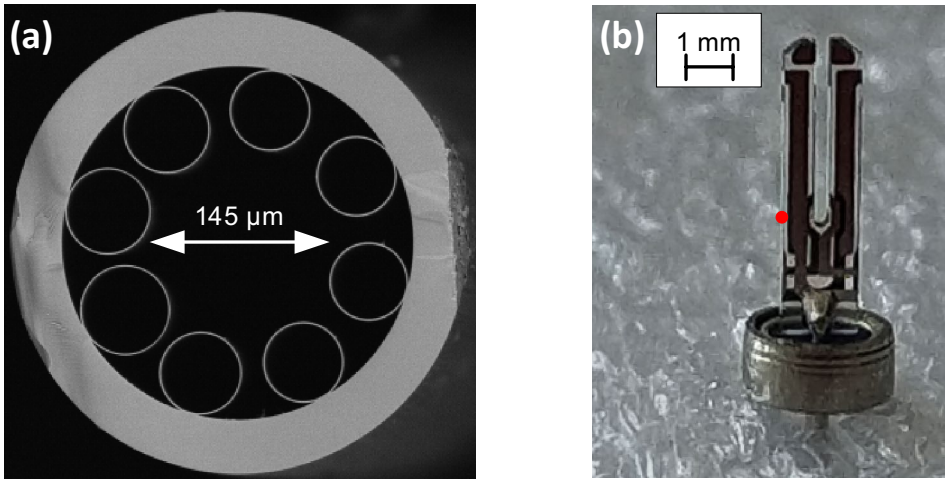

Fig. 1 **a** SEM image of the ARHCF used in the experiment as the gas absorption cell. **b** Photograph of the QTF used in the experiments with the optimal illuminated point marked with a red dot

MGC1C-P01) has a volume of 100 ml, more than 1700 times larger than ARHCF of the same length. The structure of the fiber, and hence its transmission characteristic, was designed based on the antiresonant reflecting optical waveguide (ARROW) [29] model. As a result, the selected geometric parameters of the ARHCF allowed it to guide light in two different wavelength bands, centered at 4.5 µm and 2 µm. These two spectral regions correspond to the zeroth-order and the first-order antiresonant bands of the fiber and allow covering strong transition of N_2O at 4570 nm (2188.2 cm^{-1}) and CO_2 at 2006 nm (4985.9 cm^{-1}).

The gas detection method used in the proposed ARHCF-aided sensor configuration was based on the LITES technique. A standard QTF resonator (see Fig. 1b) with an in-vacuum resonance frequency $f_r = 32.768$ (i.e., 2^{15}) kHz was used as a broadband and sensitive detector. To employ the QTF as a light detector, the aluminum shielding tube used was removed. As a result, the resonance frequency of the QTF shifts slightly, becoming $f_r = 32.756$ kHz. The QTF has been connected with a self-designed low-noise amplifier, forming a detection module (more information about the module design can be found in [30]). The module was placed on a five-axis optomechanical stage (MicroBlock Series M8T616D/M, Thorlabs Inc.), which allowed its precise alignment with respect to the ARHCF end facet. The structure of the QTF was not modified and its surface was covered with a highly reflective silver contact pattern. Hence, to obtain optimal signal level, it was necessary to align the QTF to illuminate non-silver covered areas of the quartz crystal. The position of the incident beam is crucial to obtain the highest possible signal-to-noise ratio (SNR) in the LITES technique. As reported in [31, 32], the position of the beam will determine the strength of the QTF oscillations and thus the amplitude of the generated electrical signal. Furthermore, the position of the incident beam can also affect the level of thermal noise generated by the QTF [31, 33] and this fact was also taken into account during the determination of the optimal illuminated spot of the QTF. This optimal point was established based on the procedure described in [29–32] and marked as a red dot in Fig. 1b.

2.2 Experimental setup

The sensor experimental setup is schematically depicted in Fig. 2.

The target molecules were efficiently excited inside the ARHCF's core exploiting a quantum cascade laser (QCL, HHL-961, Alpes Lasers) operating at 2188.2 cm^{-1} and a distributed feedback diode laser (DFB, EP2004-0-DM-B06-FM, Eblana) with emission centered at 4985.9 cm^{-1}, matching the selected transitions of N_2O and CO_2, respectively. To target the selected absorption lines, the QCL was operated at 17 °C with a DC driving current of 200 mA and the DFB laser temperature was set at the 19 °C with a DC driving current of 100 mA. These parameters were controlled by commercially available controllers (Thorlabs ITC4002QCL (QCL) and ITC4020 (DFB)). The QCL polarized and collimated beam was directed through a set of silver mirrors onto a nanowire grid polarizer (WP25HB, Thorlabs Inc.), which was used to combine it with the 2 µm beam and control the intensity of the QCL beam coupled into the ARHCF. The DFB laser output was first collimated with a collimator to a diameter of 1.4 mm, and subsequently its polarization was adjusted with a half-wave plate to match the orientation axis of the polarizer, allowing for its low-loss transmission and efficient coupling to the ARHCF. Both beams were coupled to the ARHCF through a single CaF_2 lens with an antireflective coating for 2.0–5.0 µm light (focal length = 40 mm, model Thorlabs LA5370-E). The measured power of the lasers at the selected wavelengths at the fiber input was 3.5 mW and 2.3 mW, and after transmission

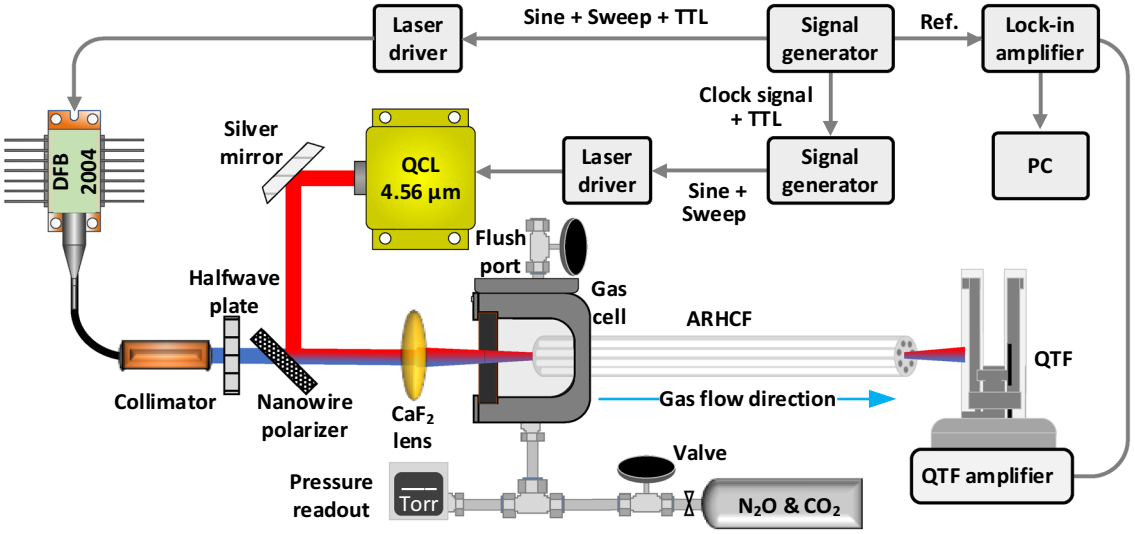

Fig. 2 Schematic of the sensor experimental setup

through the ARHCF was 2.4 mW and 1.7 mW, for the QCL and DFB lasers, respectively.

The input end facet of the ARHCF was glued to a special gas cell equipped with two gas ports that allow efficient and fast gas exchange in the fiber core. The first port was used to fill the core with the target gas mixture by a pressure-driven method [34]. The additional flush port embedded in the gas cell was used to purge the gas delivery system before each measurement. Due to that, the residual gas inside the cell could be efficiently evacuated without leaking to the hollow part of the ARHCF. This directly translated to the shorter gas-filling time of the fiber which was at the level of ~ 10 s. Furthermore, the sensor operated in the constant gas-flow mode during the measurements. To obtain this, the inlet gas pressure was set to 800 torr, while the output end face of the fiber was opened to the lab air at 760 torr pressure. This resulted in the averaged gas pressure inside the hollow part of the ARHCF at the level at 780 torr, allowing the gas sample to continuously flow through the fiber. The CaF_2 wedge (WG51050-D) on the front of the gas cell enabled efficient transmission of both laser beams through the entrance aperture of the cell and their subsequent coupling into the fiber core. The QTF used to detect the beam's amplitude was placed perpendicularly to the axis of the fiber, ~ 0.5 mm from the output facet. Due to the very low aperture of the ARHCF, no additional optical components were necessary to perform sensitive detection, which is one of the most crucial advantages of using the combination of a QTF and an ARHCF. The position of the QTF was optimized experimentally, by measuring the SNR.

The quasi-simultaneous dual-gas detection was achieved by using two independent signal generators (AFG3102C, Tektronix for the QCL and 33500B, Keysight for the DFB). Optimal sine wave modulation and sawtooth sweep voltage signals were generated and fed to the DFB and the QCL laser drivers. The generators were interconnected with a trigger signal, which enabled us to modulate and sweep the wavelengths of both lasers independently, in sequential order, to recover the absorption lines of CO_2 and N_2O separately. Both generators were synchronized to a common clock to ensure relative phase stability. More about the absorption line scanning procedure can be found in the next subsection.

To conveniently retrieve spectroscopic information in the developed LITES sensor, the second harmonic-based (2*f*) detection scheme was implemented, commonly used in the wavelength modulation spectroscopy (WMS) technique [35]. This was achieved by modulating the wavelengths of the lasers with sine wave signals. The frequency of the modulation was set to half of the resonance frequency of the QTF ($f_{mod} = f_r/2$). The electrical signal generated by the QTF was amplified with a self-made transimpedance amplifier, filtered and directed to a digital lock-in amplifier (MFLI, Zurich Instruments), which demodulated the signal at f_{mod}. With the aid of the MFLI-implemented data processing software, it was possible to clearly observe and record the measured signals.

2.3 Operating principle of quasi-simultaneous gas sensing

The operation principle of the proposed sensor configuration is based on a quasi-simultaneous detection of two gases characterized by strong transitions in two different wavelength regions. Simultaneous detection of multiple gasses is not possible due to the high Q-factor of the QTF, which prohibits using frequency division-based detection [36],

unless using properly designed custom QTF [11]. Therefore, to efficiently record spectroscopic signals from both gases inside the ARHCF-based absorption cell within a single measurement cycle, a low-frequency wavelength sweep of lasers was implemented. The optimal duration of the sweep was 5 and 4 s for the QCL and DFB lasers, respectively, which enabled us to register the entire 2*f* signal spectra for each gas. Each gas absorption spectrum was measured independently, in sequence, by turning off the laser which was not used in its part of the measurement cycle. To achieve this, the arbitrary function generators used were triggered with a TTL signal, from each other. The control scheme for this part of the system is presented in Fig. 3. In the generator 1 (G1), the sweep signal was generated at channel 1 (CH1) and the sine wave modulation signal was generated at the second channel (CH2) and added internally to the CH1 output. CH1 electric signal was fed to the modulation input of the QCL. A TTL signal from G1 was connected to the trigger input of G2. When G1 sweeps the wavelength of the QCL, the G2 turns off the DFB laser. After G1 has ended its cycle, the TTL signal triggers G2 to generate a sinewave modulation and low-frequency sawtooth ramp signals to probe the CO_2 absorption line with the DFB laser. Due to this approach, two lasers different in wavelength can effectively excite the molecules of each target gas within a single measurement cycle, hence allowing for quasi-simultaneous operation principle of the sensor. Because of the high material absorption of quartz in the mid-IR, the QCL laser was kept at a DC output power (no modulation) during the CO_2 measurement. This allowed us to avoid periodic temperature change of the QTF structure, which can result in a thermally-induced parasitic offset in the measured spectroscopic signal that negatively impact the sensitivity of the sensor in this regime. The G1 and G2 were synchronized with respect to each to avoid uncontrolled phase changes in the measured 2f signals during switching between the lasers. Therefore, G1 was used as the external synchronization source (clock) for G2, which fulfilled the aforementioned requirement. The sine wave modulation output of the G1 was also used as the frequency reference for the MFLI, which enables it to efficiently demodulate and further process the spectroscopic signals registered by the QTF.

3 System characterization

3.1 Optimization of sensor parameters

One of the frequently used methods to recover the spectroscopic signal in the LITES technique is to use the 2f detection scheme [33, 37, 38]. In this approach, the measured signal is analyzed at the second harmonic of the applied sine wave modulation frequency, which is chosen to match the resonance response of the QTF. Therefore, it is mandatory to experimentally determine the resonance frequency of the QTF, which will be used as a reference for proper adjustment of the modulation parameters and subsequent analysis of the spectroscopic signals with the aid of a lock-in amplifier. The measurements were conducted by filling the ARHCF-based absorption cell with a 25 ppmv N_2O:N_2 sample, which was prepared using a commercial gas mixer (Environics 4000) from a reference gas mixtures of 1% N_2O concentration and pure N_2 provided by Air Liquide. The average pressure of gas in the fiber was approximately 780 torr. As the response frequency is determined by the design of the QTF and is not affected by the wavelength of the exciting laser source, the experiment was performed with the QCL laser. During the measurements, the QCL was modulated with a sine wave signal with an amplitude of 180 mV (optimized further as described below), which in this particular case was generated by the MFLI lock-in amplifier. Thanks to the built-in function of the MFLI allowing for continuous sweeping of the sine wave modulation frequency, it was possible to accurately measure the response of the QTF over the selected frequency range. The MFLI was set to register the amplitude of the signal at the second harmonic of the applied modulation

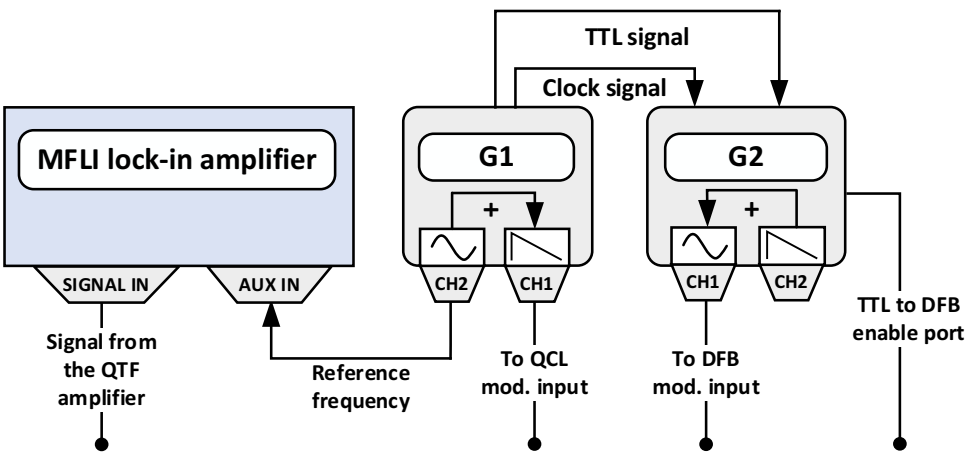

Fig. 3 Schematic of the control block of the lasers and spectroscopic signal acquisition in a quasi-simultaneous measurement mode. *G1*, *G2* arbitrary function generators, *CH1*, *CH2* output channels of the generators, *QCL* quantum cascade laser, *DFB* distributed feedback diode laser, *QTF* quartz tuning fork

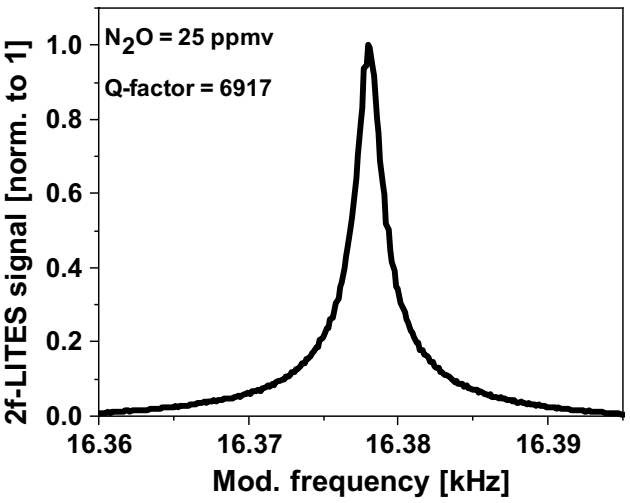

Fig. 4 Frequency response of the QTF. Amplitude of 2f LITES signal plotted as a function of the laser modulation frequency. Measurement was performed for 25 ppmv N_2O:N_2 mixture inside the ARHCF

frequency; hence the frequency scanning range had to be centered around half of the expected resonance frequency of the QTF.

In case of standard clock QTFs, the resonance frequency is in the range of 32–33 kHz. The optimal sine wave modulation frequency was determined by registering the 2*f* signal amplitudes within the selected frequency range. As shown in Fig. 4, the maximum amplitude of the 2*f* signal was observed for 16.378 kHz (corresponding to a QTF resonance frequency of 32.756 kHz), which was used in further experiments for both laser sources.

After measuring the optimal modulation frequency, the sine wave modulation amplitude (modulation depth) was experimentally determined for each laser. During the measurements, the modulation frequency was set to $f_{mod} = 16.378$ kHz for each laser, and the sine wave modulation amplitude was swept within the selected range as shown in Fig. 5. The ARHCF was filled with 25 ppmv of N_2O and 0.75% CO_2 in N_2 for each measurement, respectively. The MFLI was set to register amplitudes of the 2f

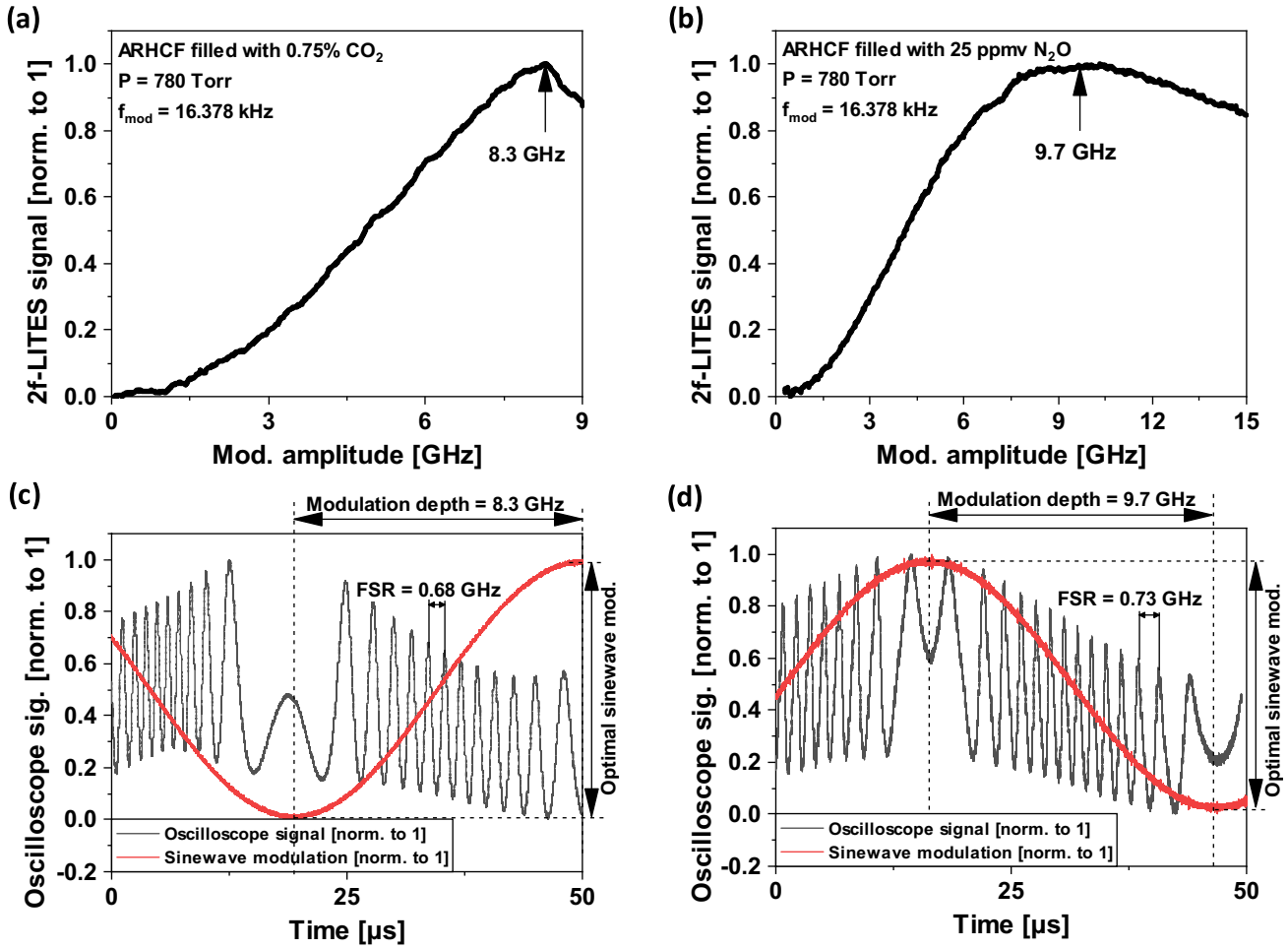

Fig. 5 Amplitude of 2f-LITES signal as a function of modulation depth for: **a** CO_2 and **b** N_2O detection. Characterization of modulation depth in GHz using germanium etalon for **c** near-infrared CO_2 detection **d** mid-infrared N_2O detection

signals for each measurement. The optimal sine wave modulation depth was defined as the value at which the 2f signal amplitudes reached their maximum values, as indicated in Fig. 5. Additionally, the modulation depth was expressed in GHz using the technique described in [19] and shown in Fig. 5. Based on the obtained results, the optimal sine wave modulation depths were 8.3 GHz and 9.7 GHz, for CO_2 and N_2O, respectively.

3.2 Sensor performance characterization

The performance of the sensor was determined by measuring the spectroscopic signals with the ARHCF-based absorption cell filled with a mixture of 0.75% CO_2 and 25 ppmv N_2O in N_2 at an average pressure of 780 torr. The lasers were set to target the gas transitions reported in Fig. 6a, based on the HITRAN database [39, 40]. The sine wave modulation and ramp signals parameters were set to the optimal values and full 2f-LITES signal spectra for each gas were registered with the aid of the MFLI lock-in amplifier and a time constant set to 10 ms. The results shown in Fig. 6b demonstrate the ability of the sensor to efficiently detect two gases having transitions in two different spectral bands in a quasi-simultaneous mode. The small dip registered at 4 s is due to the switching between the laser scans. Furthermore, immediately after both 2f-LITES signals spectra were registered, the ARHCF was rapidly flushed with pure nitrogen (N_2) and ramp signals for both lasers were switched off, while the wavelengths of both sources were set at the absorption lines of the target gases with sine wave modulations on. The MFLI was used to record the 2f-LITES noise amplitude over time, as shown in the right part of the graph in Fig. 6b. The measured data enabled us to calculate the 1σ standard deviation (SD) of the noise and, subsequently, the signal-to-noise ratio (SNR) for 10 ms time constant. The 1σ standard deviation (SD) was 0.35 mV and SNR resulted 100 and 26.5 for N_2O and CO_2, respectively.

4 Results

4.1 Sensor linearity

The performance of the sensor and its linearity were determined by measuring full 2f-LITES signal spectra and peak amplitudes for various concentrations of N_2O and CO_2 flushing through the ARHCF absorption cell. The gas samples were obtained using a commercial gas mixer starting from a certified mixture and diluting with pure N_2. The measurement parameters were set to the optimal values. The ARHCF was flushed with pure N_2 between each measurement to ensure reliable conditions. The average pressure of the measured gas mixtures in the ARHCF was set at 780 torr for the entire experiment. The full 2*f* scans collected for various concentrations of the target analytes are plotted in in Fig. 7. In addition, a 2 ppmv N_2O:N_2 mixture was also tested, for which a 2f-LITES spectrum was recorded (see inset of Fig. 7). Despite of some level of fringe-induced noise in the registered spectrum (e.g., due to interference on the optical elements in the setup), signal for this concentration of N_2O is clearly visible and correlates with the simulated trace.

The linearity of the developed sensor was determined based on plotting the peak amplitudes of the 2f-LITES signals registered for each gas as a function of their concentration. The R^2 coefficients calculated based on the linear fit of the data points shown in Fig. 8 were 0.988 and 0.982 for N_2O and CO_2, respectively, which shows good linear characteristic of the developed sensor, similar to experiments published in [13, 41, 42].

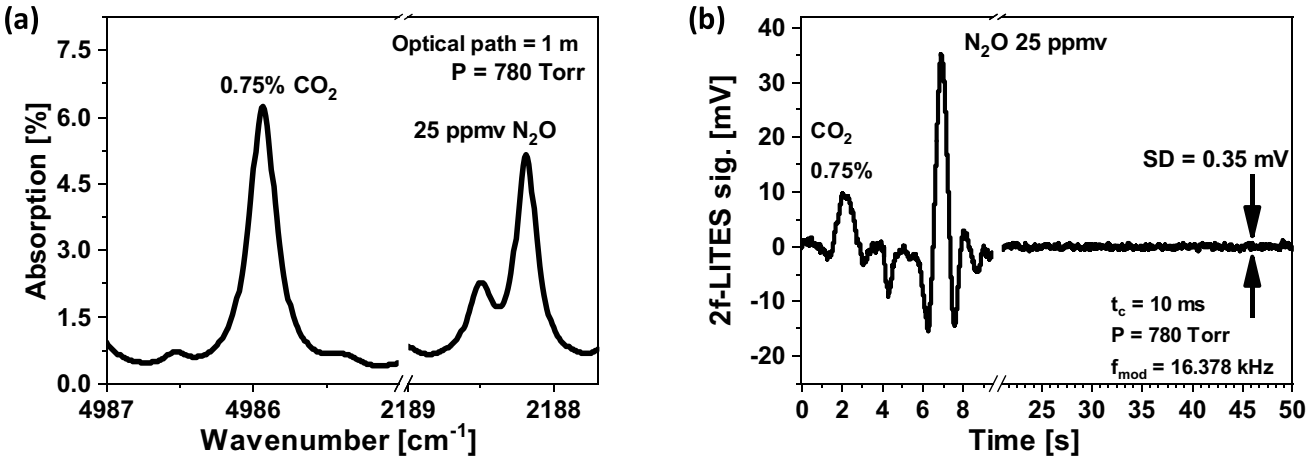

Fig. 6 **a** Absorption characteristic for mixtures of 0.75% CO_2 and 25 ppmv N_2O in N_2 (simulation based on HITRAN database [39, 40]). (b) 2f-LITES signal registered for 0.75% CO_2 and 25 ppmv N_2O in N_2, followed by a noise measurement with pure N_2 in the ARHCF gas cell

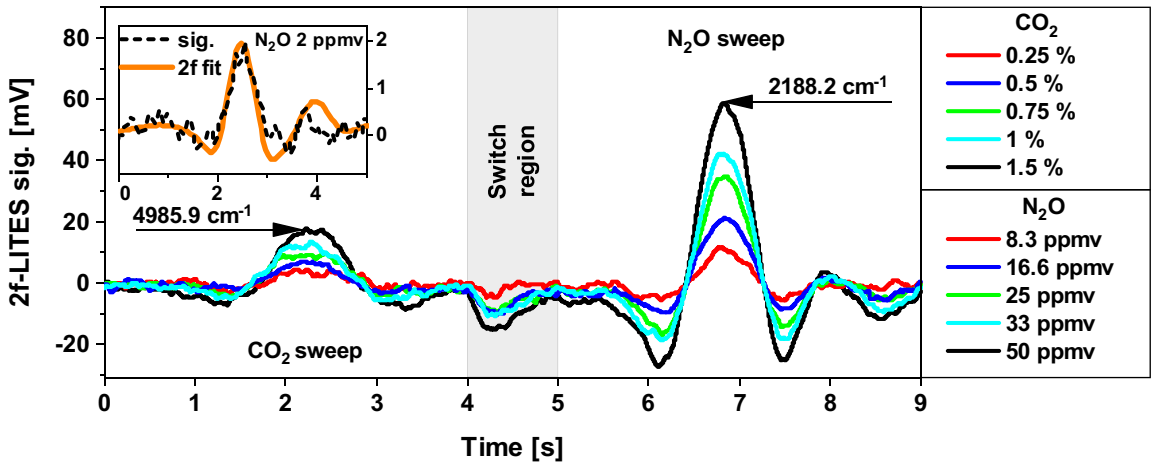

Fig. 7. 2f-LITES signals registered for various concentrations of the N_2O and CO_2 in N_2 mixtures in 1 m ARHCF. Inset shows a measurement of 2 ppmv N_2O in the N_2 mixture. The orange fit represents a signal simulated based on data from HITRAN [39, 40]

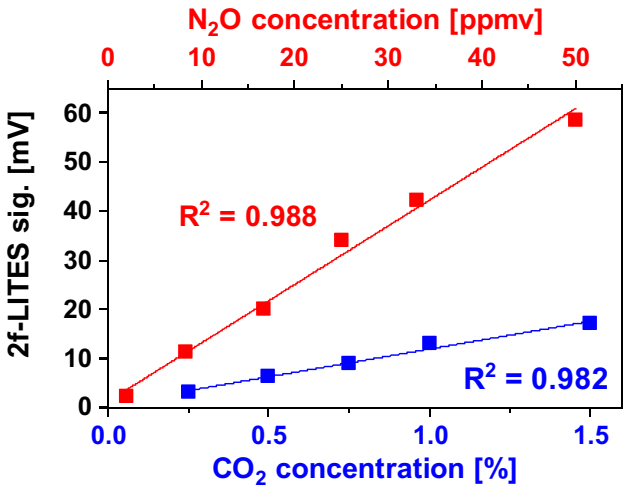

Fig. 8. 2f-LITES signal amplitudes plotted as functions of gas concentrations. Linear fits along with the calculated R^2 values are shown on the graphs

4.2 Sensor detection limit

The sensor performance was determined based on the Allan-Werle deviation analysis [43] calculated from the 2f-LITES noise signal registered for 1500 s. During this measurement, the ARHCF was flushed with N_2 at an average pressure of 780 torr.

To fully evaluate the noise contribution in the sensor, the 2f-LITES noise amplitude was registered for three cases: (a)—DFB laser ON with modulation and QCL ON with DC current, (b)—only the QCL ON with modulation and (c)—both lasers OFF. During measurement, the lasers were tuned to the center of the selected gas transitions, with no additional wavelength stabilization used. The LIA time constant was set to 10 ms. The results are plotted in Fig. 9.

The Allan–Werle deviation for each considered case was calculated based on the above presented data and plotted in Fig. 10. The minimum detection limit (MDL) of the N_2O sensor was ~ 165 ppbv and ~ 40 ppbv for 1 and 50 s of integration time, respectively. This corresponds to the noise equivalent absorption coefficient (NEA) of $\sim 8.6 \times 10^{-7}$ cm^{-1} for an integration time of 50 s. According to the data shown in Fig. 10b, the MDL for CO_2 detection was ~ 165 ppmv and ~ 20 ppmv for 1 s and 100 s, respectively, resulting in NEA of $\sim 1.7 \times 10^{-6}$ cm^{-1}. Furthermore, it can be seen that the obtained MDLs are close to the ultimate detection limits of the sensor, which depend mainly on the noise generated by the QTF electronics.

The results are at a level comparable to those achievable in similar LITES systems [31, 44–46]. We expect that the detection capacity of the sensor could be increased with further optimization of the QTF electronics, exploitation of custom QTFs optimized for LITES [37, 47] and implementation of the additional, active stabilization of the lasers wavelengths.

5 Discussion

In this work, we demonstrated a quasi-simultaneous detection of two gases in the near- and mid-IR spectral bands in a sensor configuration combining the advantages and unicity of an ARHCF-based gas absorption cell and the LITES technique. The proposed novel sensor configuration reached a detection limit of ~ 40 ppbv and ~ 20 ppmv for N_2O and CO_2, respectively. This corresponds to an NEA of $\sim 8.6 \times 10^{-7}$ cm^{-1} and $\sim 1.7 \times 10^{-6}$ cm^{-1} for N_2O

and CO_2, respectively. The detection performances of the presented sensor are comparable to those of LITES gas detectors previously reported in the literature, as indicated in Table 1. The lowest NEA values reported in refs [48,

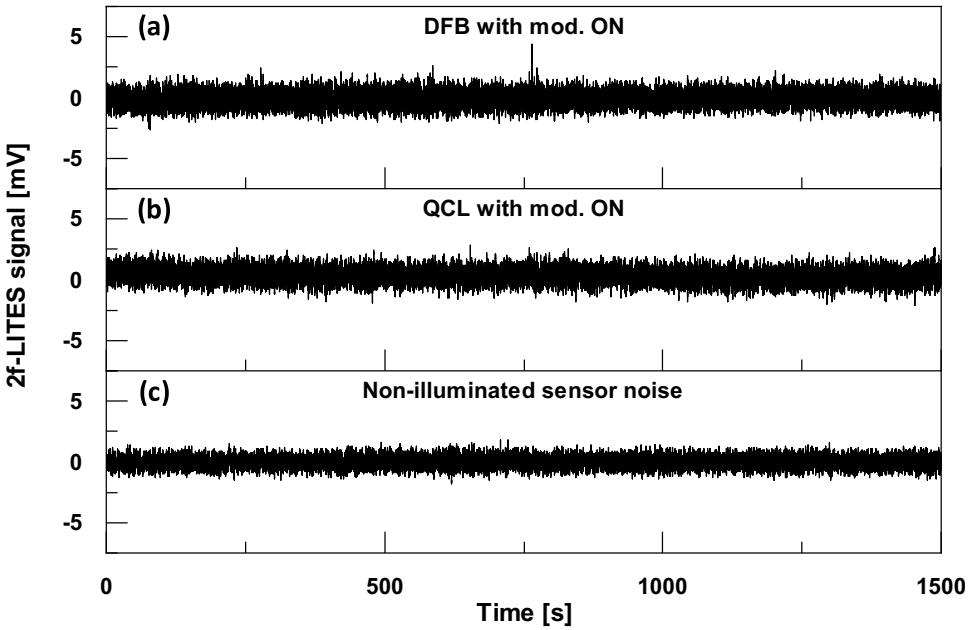

Fig. 9. 2f-LITES signal registered with N_2 flowing through the sensor (780 torr average pressure) for: **a** DFB diode with optimal 2f modulation and non-modulated QCL turned ON; **b** QCL laser source with optimal 2f modulation turned ON and DFB laser OFF; **c** non-illuminated QTF

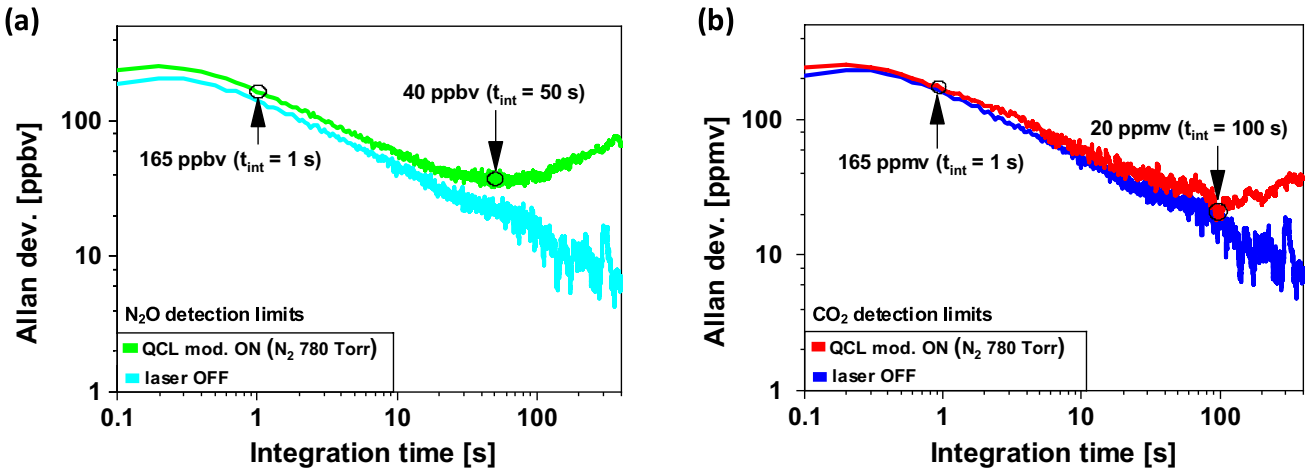

Fig. 10 Allan deviation plots calculated from the noise registered with N_2 flowing through the fiber for estimations of **a** N_2O detection limits (QCL mod. turned on). **b** CO_2 detection limits (DFB mod. turned on)

Table 1 Performance comparison of LITES gas sensors

Method	Optical path	Gas	MDL	NEA [cm^{-1}]	Refs.
LITES	20 cm	C_2H_2 (6534.37 cm^{-1})	718 ppbv	4.4×10^{-7}	[13]
LITES	30 cm	CH_4 (6046.95 cm^{-1})	48.8 ppmv	1.5×10^{-5}	[31]
OA-CETES	15 m	H_2O (7306.75 cm^{-1})	8.7 ppmv	3.0×10^{-6}	[32]
LITES	10.13 m	CO (2183.41 cm^{-1})	0.75 ppbv	3.5×10^{-8}	[48]
LITES	40 m	HCl (5747.12 cm^{-1})	148 ppbv	6.7×10^{-8}	[49]
LITES	1 m	N_2O (2188.2 cm^{-1}) CO_2 (4985.9 cm^{-1})	40 ppbv 20 ppmv	8.6×10^{-7} 1.7×10^{-6}	This paper

49] have been achieved implementing a multipass cell to enhance the optical path length and, thereby, increasing the complexity of the sensors setup, making them more sensitive to vibration and thermal effect and consequently their implementation on-field.

Conversely, the complexity of the sensor is significantly reduced if using an ARHCF as an absorption cell instead of a multipass cell. Another advantage of using an ARHCF in the sensor results from a small numerical aperture of the fiber equal to 0.03, which enables directly illuminating the selected area of the QTF without the need of using additional optics. The reduction of optical components in the sensor setup should probably lead to a less complex and more robust design with potentially increased immunity to vibrations and temperature changes [19, 50]. The ARHCF-based absorption cell can be extremely lightweight, which, combined with the ability to bend and coil the fiber, should enable the design of very compact and efficient gas sensors. Furthermore, due to the extremely small volume of the ARHCF in the range of µl, this type of absorption cell is ideally suited for applications requiring probing low-volume gas samples.

Although the detection performance of the designed sensor is comparable with similar configuration previously published, there is room for further improvement. Firstly, the long-term stability of the sensor could be significantly enhanced by introducing an active stabilization system of the lasers emission wavelength, which could be based on the use of PID controllers [51]. Further optimization in the ARHCF design, allowing for pure single-mode guidance, should result in reduction of the negative impact of the intermodal interference presented in the near-IR band, which is not the fundamental transmission window of the employed fiber. Improvement in the design of the QTF electronics aimed on reducing its noise should have an observable impact on sensor sensitivity, as well as the application of QTF properly designed for LITES [52] that could also allowed simultaneous dual gas detection [53]. More complex steps could involve building the sensors in a configuration allowing low pressure operation [44]. The above-mentioned improvements will be investigated in future experiments.

Author contributions PB: Conceptualization; PB, PJ, KK: Data curation; PB, PJ, KK: Formal analysis; KK, PJ: Funding acquisition; PB: Investigation; PB, PJ, KK: Methodology; KK, PJ: Project administration; KK, PJ, PP, WB: Resources; KK, PJ: Supervision; PB, PJ, KK: Validation; PB: Visualization; PB, PJ, KK: Writing – original draft; PB, PJ, KK, VS: Writing – review & editing.

Funding This work was supported by the National Science Centre, Poland under "M-ERA.NET 2 Call 2019" grant number 2019/01/Y/ST7/00088.

Data availability Data underlying the results presented in this paper are not publicly available at this time, but may be obtained from the authors upon reasonable request.

Declarations

Conflict of interest The authors declare that they have no known competing financial interests or personal relationships that could have appeared to influence the work reported in this paper. The authors declare no conflicts of interests.

References

1. D.M. Bailey, E.M. Adkins, J.H. Miller, Appl. Phys. B **123**, 245 (2017)
2. Y. Guo, X. Qiu, N. Li, S. Feng, T. Cheng, Q. Liu, Q. He, R. Kan, H. Yang, C. Li, Infrared Phys. Technol. **105**, 103153 (2020)
3. J. Wojtas, Sensors **15**, 14356 (2015)
4. C. Li, C. Zheng, L. Dong, W. Ye, F.K. Tittel, Y. Wang, Appl. Phys. B **122**, 185 (2016)
5. J. Shemshad, S.M. Aminossadati, M.S. Kizil, Sens. Actuators B Chem. **171–172**, 77 (2012)
6. A. Karpf, G.N. Rao, Appl. Opt. **48**, 408 (2009)
7. D.R. Herriott, H.J. Schulte, Appl. Opt. **4**, 883 (1965)
8. J. Xia, C. Feng, F. Zhu, S. Ye, S. Zhang, A. Kolomenskii, Q. Wang, J. Dong, Z. Wang, W. Jin, H.A. Schuessler, Sens. Actuators B Chem. **334**, 129641 (2021)
9. S.C. Shen, Microelectron. J.. J. **25**, 713 (1994)
10 A.A. Kosterev, Y.A. Bakhirkin, R.F. Curl, F.K. Tittel, Opt. Lett. **27**, 1902 (2002)
11. P. Patimisco, G. Scamarcio, F.K. Tittel, V. Spagnolo, Sensors **14**, 6165 (2014)
12 Y. Hu, S. Qiao, Y. He, Z. Lang, Y. Ma, Opt. Express **29**, 5121 (2021)
13 Y. Ma, Y. He, Y. Tong, X. Yu, F.K. Tittel, Opt. Express **26**, 32103 (2018)
14. A. Sampaolo, P. Patimisco, M. Giglio, A. Zifarelli, H. Wu, L. Dong, V. Spagnolo, Anal. Chim. ActaChim. Acta **1202**, 338894 (2022)
15. Y. Ma, Y. Hu, S. Qiao, Y. He, F.K. Tittel, Photoacoustics **20**, 100206 (2020)
16. P. Jaworski, Sensors **21**, 5640 (2021)
17 M. Nikodem, G. Gomółka, M. Klimczak, D. Pysz, R. Buczyński, R. Buczyński, Opt. Express **27**, 36350 (2019)
18. C. Yao, M. Hu, A. Ventura, J. G. Hayashi, F. Poletti, W. Ren, J. Lightw. Technol. **39**, 5662–5668 (2021). https://doi.org/10.1109/JLT.2021.3088140
19. P. Jaworski, K. Krzempek, P. Kozioł, D. Wu, F. Yu, P. Bojęś, G. Dudzik, M. Liao, J. Knight, K. Abramski, Opt. Laser Technol. **147**, 107638 (2022)

20. M. Nikodem, G. Gomółka, M. Klimczak, D. Pysz, R. Buczyński, Opt. Express **27**, 14998 (2019)
21. P. Jaworski, P. Kozioł, K. Krzempek, D. Wu, F. Yu, P. Bojęś, G. Dudzik, M. Liao, K. Abramski, J. Knight, Sensors **20**, 3813 (2020)
22. C. Yao, S. Gao, Y. Wang, P. Wang, W. Jin, W. Ren, IEEE Sens. J. **20**, 12709 (2020)
23 C. Yao, S. Gao, Y. Wang, P. Wang, W. Jin, W. Ren, J. Lightw. Technol. **38**, 2067 (2020)
24. P. Jaworski, K. Krzempek, G. Dudzik, P.J. Sazio, W. Belardi, Opt. Lett. **45**, 1326 (2020)
25. M. Hu, A. Ventura, J.G. Hayashi, F. Poletti, S. Yao, W. Ren, Sens. Actuators B Chem. **363**, 131774 (2022)
26. K. Krzempek, P. Jaworski, P. Kozioł, W. Belardi, Sens. Actuators B Chem. **345**, 130374 (2021)
27 P. Zhao, H.L. Ho, W. Jin, S. Fan, S. Gao, Y. Wang, P. Wang, Opt. Lett. **45**, 5660 (2020)
28. P. Zhao, Y. Zhao, H. Bao, H.L. Ho, W. Jin, S. Fan, S. Gao, Y. Wang, P. Wang, Nat. Commun.Commun. **11**, 847 (2020)
29 N.M. Litchinitser, A.K. Abeeluck, C. Headley, B.J. Eggleton, Opt. Lett. **27**, 1592 (2002)
30. P. Bojęś, P. Pokryszka, P. Jaworski, F. Yu, D. Wu, K. Krzempek, Sensors **22**, 5504 (2022)
31 L. Hu, C. Zheng, Y. Zhang, J. Zheng, Y. Wang, F.K. Tittel, Opt. Lett. **45**, 1894 (2020)
32. K. Zheng, C. Zheng, C. Zheng, L. Hu, G. Guan, Y. Ma, F. Song, Y. Zhang, Y. Zhang, Y. Wang, F.K. Tittel, Opt. Express **29**, 23213 (2021)
33. L. Hu, C. Zheng, M. Zhang, K. Zheng, J. Zheng, Z. Song, X. Li, Y. Zhang, Y. Wang, F.K. Tittel, Photoacoustics **21**, 100230 (2021)
34. P. Bojęś, P. Jaworski, K. Krzempek, Z. Malecha, F. Yu, D. Wu, P. Kozioł, G. Dudzik, M. Liao, K. Abramski, Opt. Laser Technol. **152**, 108157 (2022)
35. G.B. Rieker, J.B. Jeffries, R.K. Hanson, Appl. Opt. **48**, 5546 (2009)
36. X. Tian, Y. Cao, J. Chen, K. Liu, G. Wang, T. Tan, J. Mei, W. Chen, X. Gao, Sensors **19**, 820 (2019)
37. S.D. Russo, S.D. Russo, A. Zifarelli, A. Zifarelli, P. Patimisco, P. Patimisco, A. Sampaolo, A. Sampaolo, T. Wei, H. Wu, L. Dong, L. Dong, V. Spagnolo, V. Spagnolo, V. Spagnolo, Opt. Express **28**, 19074 (2020)
38. Y. Ma, Front. Phys. **8** (2020). https://www.frontiersin.org/articles/10.3389/fphy.2020.00268/full
39. I.E. Gordon, L.S. Rothman, R.J. Hargreaves, R. Hashemi, E.V. Karlovets, F.M. Skinner, E.K. Conway, C. Hill, R.V. Kochanov, Y. Tan, P. Wcisło, A.A. Finenko, K. Nelson, P.F. Bernath, M. Birk, V. Boudon, A. Campargue, K.V. Chance, A. Coustenis, B.J. Drouin, J.-M. Flaud, R.R. Gamache, J.T. Hodges, D. Jacquemart, E.J. Mlawer, A.V. Nikitin, V.I. Perevalov, M. Rotger, J. Tennyson, G.C. Toon, H. Tran, V.G. Tyuterev, E.M. Adkins, A. Baker, A. Barbe, E. Canè, A.G. Császár, A. Dudaryonok, O. Egorov, A.J. Fleisher, H. Fleurbaey, A. Foltynowicz, T. Furtenbacher, J.J. Harrison, J.-M. Hartmann, V.-M. Horneman, X. Huang, T. Karman, J. Karns, S. Kassi, I. Kleiner, V. Kofman, F. Kwabia-Tchana, N.N. Lavrentieva, T.J. Lee, D.A. Long, A.A. Lukashevskaya, O.M. Lyulin, VYu. Makhnev, W. Matt, S.T. Massie, M. Melosso, S.N. Mikhailenko, D. Mondelain, H.S.P. Müller, O.V. Naumenko, A. Perrin, O.L. Polyansky, E. Raddaoui, P.L. Raston, Z.D. Reed, M. Rey, C. Richard, R. Tóbiás, I. Sadiek, D.W. Schwenke, E. Starikova, K. Sung, F. Tamassia, S.A. Tashkun, J. Vander Auwera, I.A. Vasilenko, A.A. Vigasin, G.L. Villanueva, B. Vispoel, G. Wagner, A. Yachmenev, S.N. Yurchenko, J. Quant. Spectrosc. Radiat. Transf.Spectrosc. Radiat. Transf. **277**, 107949 (2022)
40. https://hitran.iao.ru
41. Y. Mi, Y. Ma, Sensors **21**, 4548 (2021)
42. X. Liu, S. Qiao, G. Han, J. Liang, Y. Ma, Photoacoustics **28**, 100422 (2022)
43. P. Werle, R. Mücke, F. Slemr, Appl. Phys. B **57**, 131 (1993)
44. Y. He, Y. Ma, Y. Tong, X. Yu, F.K. Tittel, Opt. Lett. **44**, 1904 (2019)
45. H. Zheng, H. Lin, L. Dong, Z. Huang, X. Gu, J. Tang, L. Dong, W. Zhu, J. Yu, Z. Chen, Appl. Sci. **9**, 4021 (2019)
46 X. Liu, Y. Ma, Chin. Opt. Lett. **20**, 031201 (2022)
47. T. Wei, A. Zifarelli, S. Dello Russo, H. Wu, G. Menduni, P. Patimisco, A. Sampaolo, V. Spagnolo, L. Dong, Appl. Phys. Rev. **8**, 041409 (2021)
48 S. Qiao, Y. Ma, Y. He, P. Patimisco, A. Sampaolo, V. Spagnolo, Opt. Express **29**, 25100 (2021)
49. S. Qiao, A. Sampaolo, P. Patimisco, V. Spagnolo, Y. Ma, Photoacoustics **27**, 100381 (2022)
50. P. Jaworski, K. Krzempek, P. Bojęś, D. Wu, F. Yu, Opt. Laser Technol. **156**, 108539 (2022)
51. Q. Wang, Z. Wang, W. Ren, Meas. Sci. Technol. **28**, 065102 (2017)
52. Y. Ma, Y. He, P. Patimisco, A. Sampaolo, S. Qiao, X. Yu, F.K. Tittel, V. Spagnolo, Appl. Phys. Lett. **116**, 011103 (2020)
53. A. Elefante, M. Giglio, A. Sampaolo, G. Menduni, P. Patimisco, V.M.N. Passaro, H. Wu, H. Rossmadl, V. Mackowiak, A. Cable, F.K. Tittel, L. Dong, V. Spagnolo, Anal. Chem. **91**, 12866 (2019)